Inspired Metamaterial Quad-Band Printed Inverted-F (IFA) Antenna for USB Applications

Ahmed M. Soliman [1], Dalia M. Elsheakh [2], Esmat A. Abdallah [2], and Hadia M. El-Hennawy [1]

[1] Electronics and Communication Engineering Department
Faculty of Engineering, Ain Shams University, Cairo, 11517, Egypt
ahmed.soliman2020@yahoo.com

[2] Electronics Research Institute
Cairo, 12622, Egypt
daliaelsheakh@eri.sci.eg

Abstract ― This paper presents quad-band printed inverted-F antenna that employs transmission-line based on inspired metamaterials for USB applications. The reactive loading of the printed IFA is inspired by transmission-line based metamaterials (TL-MTM), which is exploited to create a new resonant frequency while maintaining the antenna's small form-factor. The proposed USB antenna structure consists of two arms printed IFA CPW-fed loaded with two TL-MTM unit cells to achieve two operating bands with the same antenna size in addition to the two fundamental resonant frequencies of IFA arms themselves. The structure is designed to operate at LTE 11 0.9 GHz, Bluetooth 2.4 GHz, WIMAX 3.5 GHz, and WLAN 5.2 GHz. The component interaction including housing case, USB connector, and laptop device are also characterized. The design concept, a parametric study of the proposed antenna is carried out using HFSS ver. 14 and CST ver. 2014, and general design guidelines are provided. Experimental results are presented to validate the new design concept. Measurements and EM simulations are in a good agreement.

Index Terms ― High frequency structure simulator (HFSS), inspired metamaterials, inverted-F antenna (IFA), transmission-line based metamaterials (TL-MTM), universal serial bus (USB).

I. INTRODUCTION

Universal serial bus device (USB) [1] is a good candidate for data transmission in most digital devices. The challenge in designing a USB antenna is to design compact, low cost and multiband antenna to support multi standards as much as possible. Generally, the monopole antenna applied to a wireless USB dongle has dual resonances including 2.4 GHz and 5.2 GHz bands only [2-3]. A new research paper [4] supports triple band operation. These designs use traditional approach such as meander shaped slots [2], [4], and fractal shapes [3]; however, there is tradeoff between design complexity, and fabrication cost associated with multiband extension. On the other hand, the printed-F antenna offers an attractive solution for modern wireless communication systems because it has a low profile, can be etched on a single substrate and can provide the feature of broadband or multiband operation. Recently, the combination of inspired metamaterial and printed IFA has proven to be a good candidate for the design of compact multiband USB antennas [5]. Also, the transmission-line metamaterials (TL-MTM) provide a conceptual route for implementing small resonant antennas [6]-[9]. TL-MTM structures operating at resonance are first proposed in order to implement small printed antennas in [7].

In this paper, quad-band CPW fed printed IFA antenna is proposed using reactive loading, that is inspired by using the negative-refractive-index (NRI) transmission line metamaterial π unit cell [9], in order to meet the specifications of the long term evaluation LTE900 (0.9–0.96) GHz, the Wi-Fi bands (lower Wi-Fi band) of (2.4–2.48) GHz and upper Wi-Fi band of (5.2–5.25) GHz, and the WiMAX (3.5–3.6) GHz band while maintaining a small form factor for USB applications. All simulations are carried out using the EM commercial simulator, HFSS which is based on finite element method.

The rest of the paper is organized as follows: in Section II, the design and simulation of the proposed antenna is described. Section III discussed the components interaction. Section IV explains the experimental results and discussion. Section V concludes and summarized the features of the proposed

Submitted On: August 14, 2014
Accepted On: December 10, 2014

antenna.

II. ANTENNA DESIGN AND SIMULATION

Figure 1 shows the geometry of the 2D and 3D antenna, resonating at four frequency bands at 0.9, 1.8, 3.5, and 5.2 GHz, respectively. Table 1 shows the optimized dimensions of the proposed antenna. The antenna is designed on a low-cost FR4 substrate with height h = 0.8 mm, dielectric constant ε_r = 4.7 and loss tangent $tan\ \delta$ = 0.025. The antenna is fed by a CPW transmission-line, which can be easily integrated with other CPW-based microwave circuits printed on the same substrate. The CPW feed is connected to the coaxial cable through a standard 50 Ω SMA connector. The overall size of the antenna including the ground plane is 50×20×0.8 mm^3. The proposed design is via-free and can therefore be easily fabricated. The design steps and their responses are shown in Fig. 2. The reactive loading of the CPW fed IFA is inspired by transmission-line metamaterials, specifically the concept of a zero-index of refraction.

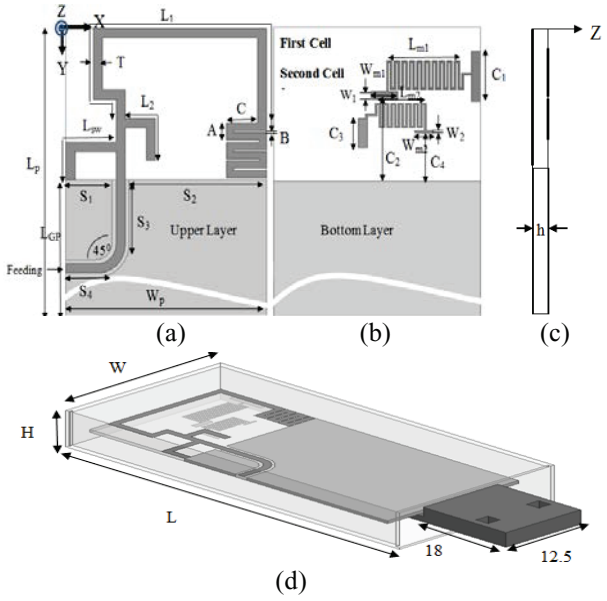

Fig. 1. Quad-band CPW fed printed IFA antenna with two metamaterial inspired unit cells: (a) top view, (b) bottom view, (c) side view, and (d) 3D schematic with housing case and USB connector.

Table 1: The dimensions of the proposed antenna (all dimensions in mm)

W_p	L_p	L_1	L_2	S_1	S_2	S_3	S_4	L_{sw}
20	50	39	6.75	4.5	14.1	7.3	3.8	9.5
L_{GP}	A	B	W_{m1}	W_{m2}	L_{m1}	L_{m2}	C_1	T
34	1.8	0.2	0.8	0.3	7.7	5.4	5.2	1
C_2	C_3	C_4	C	W	W_1	W_2	L	H
8.5	3	5	3.4	26	1	0.3	55.5	10

In order to maintain the antenna's small form-factor while achieving more operating frequencies, the CPW two IFA arms were loaded with a dual asymmetric negative-refractive-index transmission line (NRI-TL) metamaterial-based π unit cell, as shown in Fig. 3 (a). The matched dispersion characteristics of the proposed π unit cell is shown in Fig. 3 (b) [8]-[14-16] around 2.4 GHz. The structure consists of a host TL medium periodically loaded with discrete lumped element components. The unit cell was implemented at 2.4 GHz using the advanced design system (ADS) microwave circuit simulator. The impedance matching condition [8]-[14-15] has been satisfied and, therefore, the stop band has been closed. It can also be observed that at 2.4 GHz, the phase shift is 0 (balanced case).

The design flow can be described with the aid of Figs. 2 (a) to (d), and its corresponding reflection coefficient $|S_{11}|$ less than -6 dB is shown in Fig. 2 (e) as follows.

First step starts by designing the conventional CPW fed printed IFA as shown in Fig. 2 (a) to operate at 0.9 GHz, with L_1=39 mm. $|S_{11}|$ is shown as blue dashed dotted line in Fig. 2 (e).

Second step is to add the IFA second arm with L_2 = 6.75 mm as shown in Fig. 2 (b), to operate at WLAN 5.2 GHz, shown as red dashed line in Fig. 2 (e).

The resonant frequencies of first and second IFA arms can be approximately determined by [10]:

$$F \approx \frac{c}{4\sqrt{\varepsilon_{reff}}(L_i)}, \quad (1)$$

where C, L_i and ε_{reff} are the speed of light, *the IFA 1st*, *2nd* arm lengths and the effective dielectric constant, respectively.

Third step of design, shown in Fig. 2 (c), is to load the first cell to operate at 2.7 GHz, shown as dotted green line in Fig. 2 (e).

Fourth step of design, shown in Fig. 2 (d), is adding the second cell with different size to operate at WIMAX 3.5 GHz, shown as gray solid line in Fig. 2 (e). It is noticed that the resonant frequency at 2.7 GHz is reduced to be at Bluetooth 2.4 GHz, due to the coupling effect of the nearby elements. All dimensions are listed in Table 1. The two capacitors formed between the first cell, the first IFA arm and ground plane, are represented by the two lengths C_1 and C_2, respectively. The same with the second cell, the lengths C_3 and C_4 represent the two capacitors between the second cell, the first IFA arm and ground plane while the two inductors of first and second cells are represented by the two lengths meander lines, L_{m1} and L_{m2}, respectively. The length L_{m1} is represented by ten turns of 8.8 mm one turn length. The length L_{m2} is represented by seven turns of 8.8 mm one turn length. With decreasing the capacitor C_1 between the first cell and the IFA first arm, the three resonant 3.5 GHz, 2.5 GHz, and 5.2 GHz are affected, while all other parameters remain constant. The first cell is coupled to

the second cell and the IFA second arm. The same happens when decreasing the number of meander line length as shown in Fig. 4. The parameters C_1 and C_2 represent the capacitive loading (distance to ground plane), therefore the most significant effect will be capacitive. While the length L_{m1} and L_{m2} represent the inductive loading (the parameter's lengths are increased right and left without moving toward the ground plane), therefore the most significant effect will be inductive.

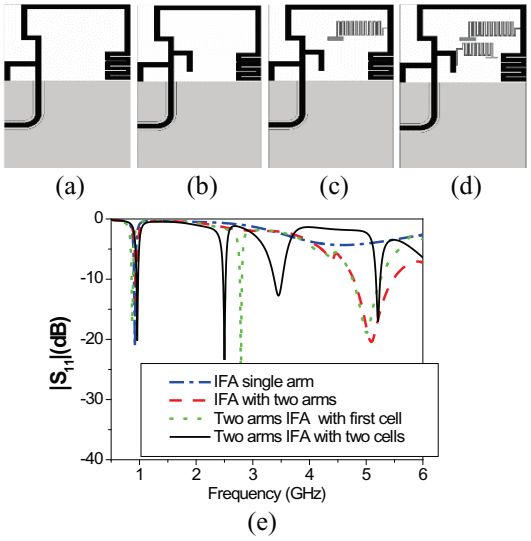

Fig. 2. (a)-(d) Design steps of the proposed quad printed-IFA, and (e) the $|S_{11}|$ design procedures of the proposed antenna.

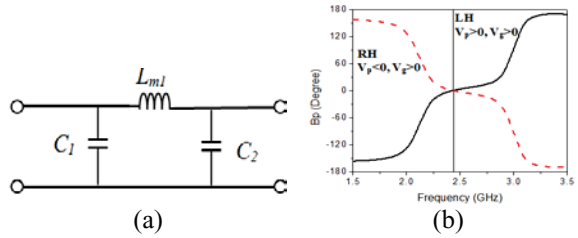

Fig. 3. (a) The equivalent circuit when the proposed antenna operates at the first arm IFA, and (b) dispersion relation calculated for the balanced first π unit cell.

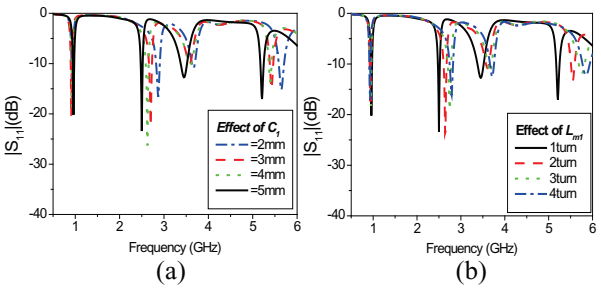

Fig. 4. Variation of $|S_{11}|$ against first cell parameters: (a) C_1, and (b) L_{m1}.

On the other hand, with decreasing the number of meander line turns and length C_3 between the second cell and IFA second arm, the resonant frequency is increased for wireless communication applications, as shown in Figs. 5 (a) and (b), while all other parameters almost remain unchanged. The same happens when increasing the length C_4 between the second cell and the IFA second arm, as shown in Fig. 5 (c). The second cell has independent tuning due to free space zone to the ground plane

Otherwise, the first cell has dependent tuning due to coupling effect with second cell and IFA second arm loading. The operations of the antenna at the four resonant frequencies are further studied using the surface current distribution, as shown in Fig. 6. In addition to the two fundamental resonant frequencies of the two IFA arms, at 0.9 GHz and 5.2 GHz, the two TL-MTM reactive loading unit cells introduce new two resonances around Bluetooth 2.4 GHz and WIMAX 3.5 GHz. At these frequencies, the antenna no longer acts as a printed IFA mode, but rather as dipole mode along the x-axis [7], as shown in Figs. 6 (b) and (c). The highest current densities mainly flow around each element that corresponds to its resonant frequency, and so is responsible for the corresponding radiations.

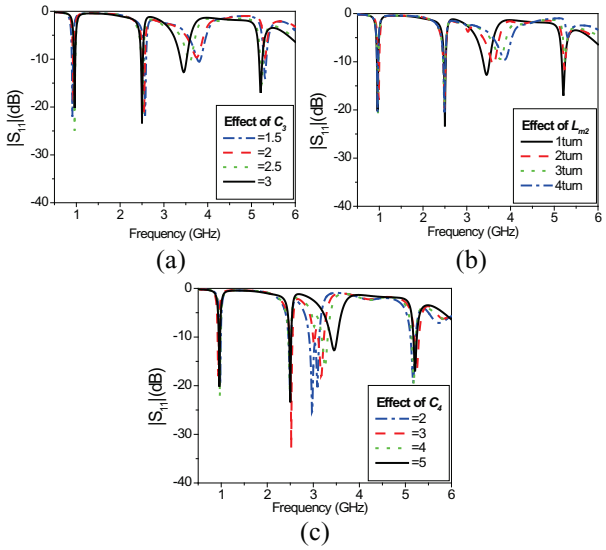

Fig. 5. Variation of $|S_{11}|$ against second cell parameters: (a) C_3, (b) L_{m2}, and (c) C_4.

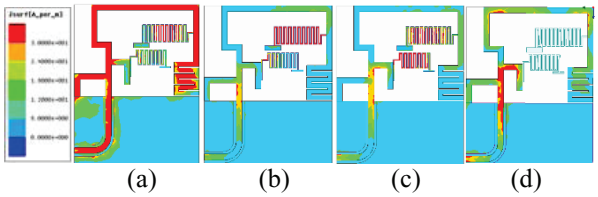

Fig. 6. The surface current distribution at: (a) 0.9 GHz, (b) 2.4 GHz, (c) 3.5 GHz, and (d) 5.2 GHz, respectively.

III. COMPONENTS INTERACTION

The whole USB structure has dimensions of 0.8×20×50 mm^3, while the USB antenna has dimensions of 0.8×20×16 mm^3. The rest of this space is used to mount the other components of the USB. Therefore, component interaction is an issue to take into account as for mobile handset [11]. This section deals with the effect of the housing case, USB connector and laptop device on the antenna performance.

Figure 7 (a) shows the geometry of the USB antenna with housing case, USB connector, and laptop device. The antenna is packaged with PVC (Polyvinyl chloride) casing materials of permittivity 4.5. The permittivity of screen, keyboard, laptop housing are 3.5, 2.25 and 3, respectively. Figure 7 (b) shows the effect on antenna reflection coefficient of the proposed antenna. To validate our results we are using another simulator, microwave studio transient solver (CST) ver. 2013, which is based on finite integral technique.

It is noticed that loading the antenna with PVC housing case, USB connector, and laptop device causes a slight shift on the frequencies at 0.9 GHz, 3.5 GHz and 5.2 GHz, but still covers the channel bandwidth of LTE, WIMAX and upper WLAN.

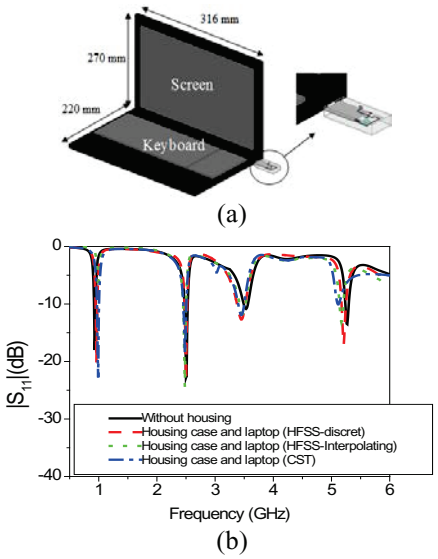

Fig. 7 (a). The HFSS proposed antenna with housing case, USB connector and laptop device, and (b) simulated $|S_{11}|$ of the proposed antenna with housing case, connector and laptop using different simulators.

In the simulation, it seems that the proposed antenna is too small with respect to the laptop. The simulation results are performed using HFSS, both solver discreet and interpolating setup solution and CST microwave studio time domain solver. HFSS and CST programs have automatic and manual adaptive meshing options. The number of mesh cells could be controlled in the antenna's area than the other areas (laptop), as shown in Table 2. As expected, there is a slight difference between both results due to different methods of meshing, as shown in Fig. 7 (b).

Table 2: Different simulator parameters

Simulator	HFSS Interpolating	HFSS Discreet	CST
Start F_o (GHz)	0.1	0.1	0.1
Stop F_o (GHz)	6	6	6
Step F_o (GHz)	0.01	0.01	0.01
No. of points	551	551	551
No. of tetra hydras	95391	195244	-
No. of mesh cells	-	-	24200079

IV. EXPERIMENTAL RESULTS AND DISCUSSION

To verify the simulated results, two proposed antennas are fabricated at C_4=5 mm and C_4=2 mm, as shown in Figs. 8 (a) and (b). The antennas are fabricated using photolithographic technique and were measured using Rohde and Schwarz ZVA67. A 50 Ω CPW feed line with a metal strip width W_s=1 mm and a gap distance W_{ss} =0.2 mm is used to excite the designed antenna. Figure 9 (a) shows the comparison between the simulated and measured reflection coefficient of the antenna. The experimental result shows good agreement with the simulated one at the target operating frequencies. Figure 9 (b) shows that the unbalanced case between the right and left handed regions [8] are appeared when decreasing the length C_4 to 2 mm, which broaden the bandwidth of the original resonant frequency of the second cell itself, covering wide bandwidth at 3 GHz.

Figure 8 (c) and Fig. 9 (c) show the fabricated USB antenna with the PVC case material and comparison between measured and simulated $|S_{11}|$, respectively. It is noticed that matching is improved by increasing the permittivity of the casing material, while the radiation efficiency is worsened. The simulated gains, radiation efficiency at each operating frequency are summarized in Table 3. The radiation efficiency was measured by using wheeler-cap method [12-13]. The average radiation efficiency is more than 75% over operating frequencies. The measured -6 dB impedance bandwidths for each resonance are suitable for the channel bandwidth of the LTE band 11 (0.9-0.96 GHz), Bluetooth (2.4-2.45 GHz), WIMAX (3.5-3.6 GHz), and upper WLAN (5.2-5.25 GHz).

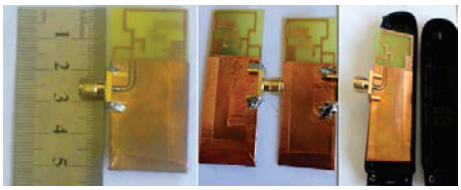

(a) (b) (c)

Fig. 8. Photos of proposed antennas (C_4=2 mm & 5 mm): (a) upper layer, (b) bottom layer, and (c) with casing material.

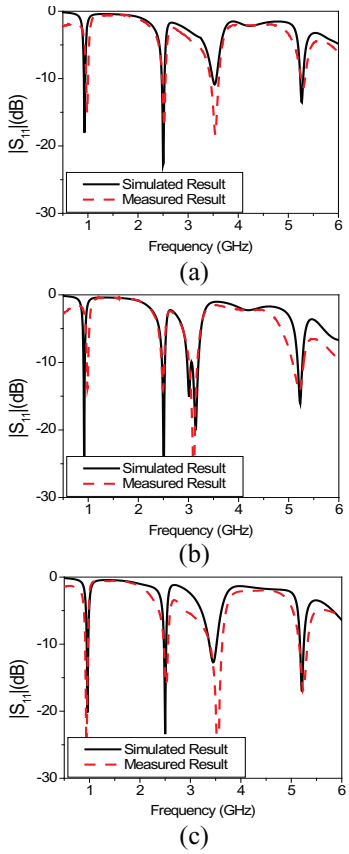

Fig. 9. Simulated and measured $|S_{11}|$ of the proposed antenna: (a) C_4=5 mm, (b) C_4=2 mm, and (c) with package of PVC casing material.

Table 3: The simulated and measured antenna parameters

Parameter \ F_o (GHz)	0.9	2.4	3.5	5.2
Sim. Gain (dBi)	2.2	2.5	2.6	2.9
Sim. Effi. (%)	65	79	85	88
Measu. Effi. (wheeler) (%)	68	81	84	86
Sim. BW (MHz) (-6 dB)	70	80	95	80
Measu. BW (MHz) (-6 dB)	70	80	90	120

The radiation patterns of the proposed antenna are measured in a Star-Lab 18 anechoic chamber, and the walls inside the chamber are covered with absorbing materials to mitigate signal reflections. The simulated and measured radiation patterns of the proposed antenna are listed in Table 4 in E-plane ($\Phi = 0^0$) and H-Plane ($\theta = 90^0$), with normalized co- and cross-polarization (E_Φ and E_θ), respectively. For almost all frequency bands, the normalized co-polarized (co-pol) patterns show nearly omni-directional radiations and their corresponding cross-polarized (x-pol) patterns exhibit monopole-like. The average difference between the co and cross levels in the main plane for most of the frequencies is higher than 10 dB, which is accepted for wireless communication. Some discrepancies between the simulated and measured results appear at certain frequencies that may be attributed to the inadequate size of the absorbers in addition to normalization error.

Table 4: Radiation patterns, simulated: black lines; measured: red lines; E_Φ: solid lines; E_θ: dotted lines at each resonant frequency; axes are shown in Fig. 1

Fo (GHz)	XZ	XY
0.9	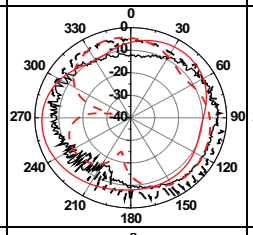	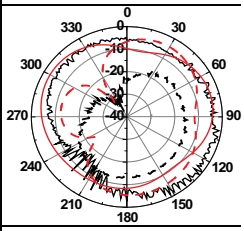
2.4	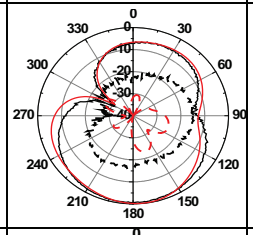	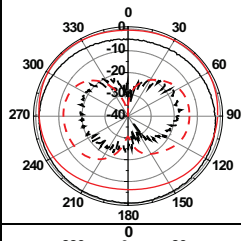
3.5	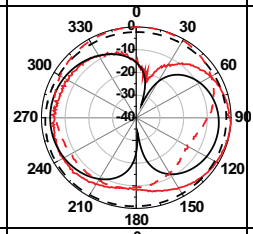	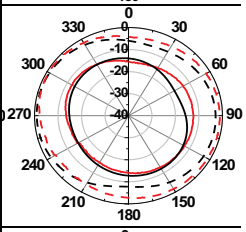
5.2	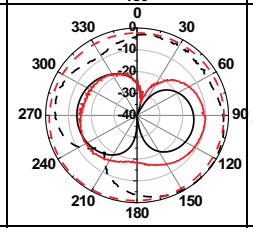	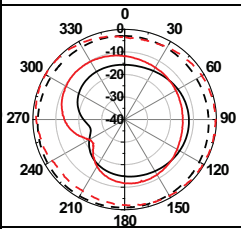

V. CONCLUSION

New quad-band USB antenna was presented in this paper. A metamaterial inspired reactive loading was used to create multiband for wireless USB applications. The theory of the proposed antenna was verified by using EM simulator and measurements. The antenna was designed to have quad-band operation covering LTE 0.9 GHz, Bluetooth 2.4 GHz, WIMAX (3.5 GHz), and upper WLAN (5.2 GHz) bands. The effect of the laptop, housing case, and USB connector is studied using different simulation programs. The results show that these components have no significant effect on the performance of the proposed antenna. The measured and simulated results were in good agreement. The proposed antenna demonstrates good gain and radiation efficiency. The radiation patterns approximate an omnidirectional pattern. These features make the antenna a good candidate for a multiband USB dongle antenna.

ACKNOWLEDGEMENTS

This research is funded by the National Telecommunication Regularity Authority, (NTRA), Ministry of Communication and Information Technology, Egypt.

REFERENCES

[1] http://en.wikipedia.org/wiki/Universal_Serial_Bus

[2] S. Lee and Y. Sung, "Multiband antenna for wireless USB dongle applications," *IEEE Antennas and Wireless Propagation Letters*, vol. 10, pp. 25-28, 2003.

[3] S. Chaimool, C. Chokchal, and P. Akkrak, "Multiband loaded fractal loop monopole antenna for USB dongle applications," *IET Electronics Letters*, vol. 48, pp. 388-390, 2012.

[4] Y. Park, D. Kang, and Y. Sung, "Compact folded tri-band monopole antenna for USB dongle applications," *IEEE Antennas and Wireless Propagation Letters*, vol. 11. pp. 228-231, 2012.

[5] A. Soliman, D. E-Sheakh, and E. A. Abdallah, "Compact independent tri-band printed-IFA loaded with inspired metamaterial for wireless communication applications," *17th European Conference on antenna and Propagation (EUCAP) Conference*, pp. 931-934, 2013.

[6] G. Eleftriades, A. Lyar, and P. Kamar, "A compact tri-band monopole antenna with single-cell metamaterial loading," *IEEE Trans. Antennas Propagat*., vol. 58, pp. 1031-1038, Apr. 2010.

[7] G. Eleftriades and K. Balmain, *Negative-Refraction Metamaterials: Fundamental Principles and Applications*, Hoboken/Piscataway, NJ: Wiley/IEEE Press, 2005.

[8] G. Eleftriades, A. Grbica, and M. Antoniades, "Compact linear lead/lag metamaterial phase shifters for broadband applications," *IEEE Antennas and Wireless Propagation Letters*, vol. 2, pp. 104-107, 2003.

[9] M. Antoniades and G. Eleftriades, "A folded-monopole model for electrically small NRI-TL metamaterial antennas," *IEEE Antennas and Wireless Propagation Letters*, vol. 7, pp. 425-428, 2008.

[10] D. Elesheakh, H. Elsadek, and H. Ghali, "Single feed compact quad-band PIFA antenna for wireless communication applications," *IEEE Trans. Antennas Propagat*., vol. 53, pp. 36-43, 2005.

[11] K. Wong and H. Chang, "Surface-mountable EMC monopole chip antenna for WLAN operation," *IEEE Trans. Antennas Propagat*., vol. 54, pp. 1100-1104, 2006.

[12] H. Wheeler, "The radian sphere around a small antenna," *Proceedings of the IRE*, vol. 47, pp. 1325-1331, 1959.

[13] W. Mckinzie, "A modified wheeler cap method for measuring antenna efficiency," *Proceedings of the IEEE Symp. Antennas and Propag*., pp. 542-545, 1997.

[14] T. Zvolensky, J. A. Laurinaho, C. R. Simovski, and A. V. Räisänen, "A systematic design method for CRLH periodic structures in the microwave to millimeter-wave range," *IEEE Trans. Antennas Propagat*., vol. 62, no. 8, pp. 4153-4161, Aug. 2014.

[15] A. Lai, T. Itoh, and C. Caloz, "Composite right/left-handed transmission line metamaterials," *IEEE Microw. Mag.*, vol. 5, no. 3, pp. 34-50, Sep. 2004.

[16] C. Caloz and T. Itoh, *Electromagnetic Metamaterials: Transmission Line Theory and Microwave Applications*, Hoboken, NJ, USA: Wiley, ch. 3, 5, and 6, 2006.

Ahmed M. Soliman was born in Cairo in 1987. He received the B.Sc. degree (with honors) in Electrical and Communication Engineering from Shoubra Faculty of Engineering, Zagazig University, Cairo, Egypt, in 2009. Currently, he is working towards the M.Sc. degree at the Faculty of Engineering, Ain Shams University. Since his graduation, he was appointed as an R.A. by the Electronics Research Institute, Microstrip Department, Giza, Egypt. His graduation project was to design a communication system for cube satellite under the supervision of the National Authority for Remote Sensing and Space Sciences (NARRS). He and his graduation projects team received the Information

Technology Industry Development Agency Award, the 2009 Young Investigator Award, and Giza Systems School of Technology scholarship Award.

Dalia M. Elsheakh born in Giza, Egypt, in 1976. She received the B.S., M.S., and Ph.D. degrees in Electrical and Communication Engineering from Ain Shams University, Cairo, Egypt, in May 1998, 2004 and 2010 respectively. M.Sc. title, "The Design of Microstrip PIFA Antennas for Mobile Handsets" and Ph.D. entitled, "Electromagnetic Band-Gap (EBG) Structure for Microstrip Antenna Systems (Analysis and Design)". From 2000 to 2004 she was a Research Assistant and from 2004 to 2010 she has been an Assistant Researcher with the Microstrip Department, Electronic Research Institute. She has been an Assistant Professor with the Microstrip Department. 2014 she has been an international visitor in Hawaii Center for Advanced Communications (HCAC).

Esmat A. Abdallah graduated from the Faculty of Engineering and received the M.Sc. and Ph.D. degrees from Cairo University, Giza, Egypt, in 1968, 1972, and 1975, respectively. She was nominated as Assistant Professor, Associate Professor and Professor in 1975, 1980 and 1985, respectively. In 1989, she was appointed President of the Electronics Research Institute ERI, Cairo, Egypt, a position she held for about ten years. She became the Head of the Microstrip Department, ERI, from 1999 to 2006. She has focused her research on microwave circuit designs, planar antenna systems and nonreciprocal ferrite devices, and recently on EBG structures, UWB components and antenna and RFID systems.

Hadia M. El Hennawy received the B.Sc. and the M.Sc. degrees from Ain Shams University, Cairo, Egypt, in 1972 and 1976, respectively, and the Ph.D. degree from the Technische Universitat Braunschweig, Germany, in 1982. In 1982, she returned to Egypt and joined the Electronics and Communications Engineering Department, Ain Shams University, as an Assistant Professor. She was nominated an Associate Professor in 1987 and then a Professor in 1992. In 2004, she was appointed as the Vice-Dean for Graduate Study and Research. In 2005, she was appointed as the Dean of the Faculty of Engineering, Ain Shams University. She has focused her research on microwave circuit design, antennas, microwave communication and recently wireless communication. She has been the Head of the Microwave Research Lab since 1982.